

Remote synchronization reveals network symmetries and functional modules

Vincenzo Nicosia,¹ Miguel Valencia,² Mario Chavez,³ Albert Diaz-Guilera,⁴ and Vito Latora^{5,6}

¹Computer Laboratory, University of Cambridge, Cambridge CB3 0FD, United Kingdom

²Neurophysiology Laboratory, CIMA, University of Navarra, 31008 Pamplona, Spain

³CNRS UMR-7225, Hôpital de la Salpêtrière, 47 Boulevard de l'Hôpital, 75013 Paris, France

⁴Dept. de Física Fonamental, Facultat de Física, Universitat de Barcelona, E-08028 Spain

⁵School of Mathematical Sciences, Queen Mary University of London, London E1 4NS, United Kingdom

⁶Dipartimento di Fisica ed Astronomia, Università di Catania and INFN, I-95123 Catania, Italy

(Dated: November 26, 2012)

We study a Kuramoto model in which the oscillators are associated to the nodes of a complex network and the interactions include a phase frustration, thus preventing full synchronization. The system organizes into a regime of remote synchronization where pairs of nodes with the same network symmetry are fully synchronized, despite their distance on the graph. We provide analytical arguments to explain this result and we show how the frustration parameter affects the distribution of phases. An application to brain networks suggests that anatomical symmetry plays a role in neural synchronization by determining correlated functional modules across distant locations.

PACS numbers: 05.45.Xt, 89.75.Fb, 89.75.Kd

Synchronization of coupled dynamical units is an ubiquitous phenomenon in nature [1]. Remarkable examples include phase locking in laser arrays, rhythms of flashing fireflies, wave propagation in the heart, and also normal and abnormal correlations between different regions of the human brain [2–4]. In 1975 Y. Kuramoto proposed a simple microscopic model to study collective behaviors in large populations of interacting elements [5]. In its original formulation the Kuramoto model describes each unit of the system as an oscillator with a pre-assigned natural frequency, which interacts with all the other units and continuously readjusts its frequency in order to minimize the difference between its phase and the phase of all the other oscillators. This model has shown very successful in understanding the emergence of synchronization and, over the years, many variations have been considered [6–8]. Recently, the Kuramoto model has been also extended to the case where the oscillators are the nodes of a complex network [2, 9, 10], and it has been found that the topology of the interaction network has a fundamental role in the emergence and stability of synchronized states [11]. In particular, the presence of modular structures in the network has a relevant impact on the path to synchronization [12–16], so that practice, units that are spatially close to each other on the network, or belong to the same tightly connected group of nodes (module or community) [17], have a higher chance to have similar dynamics. This implies that nodes in the same structural module often share similar functions, which is a belief often supported by empirical findings [3]. However, various examples are found in nature where functional similarity is instead associated with morphological symmetry. In these cases, units with similar roles, which could potentially swap their position without altering the overall functioning of the system, appear in remote locations of the network. Some examples include corti-

cal areas in brains [18], symmetric organs in plants and vertebrates, and even atoms in complex molecules [19]. Therefore, identifying the sets of symmetric units of a complex system might be helpful to understand its organization. Finding the *global symmetries* in a graph, the so-called graph automorphism problem, is a well studied problem in graph theory, but to date it is still unknown if constructing the automorphism group of a graph is polynomial or NP-complete, even if there exist polynomial-time algorithms for graphs with bounded maximum degree [20]. Recent works have focused instead on the problem of defining and detecting *local symmetries* in complex networks [21, 22]. Nevertheless, the interplay between the structural symmetries of networks and the dynamical properties of processes occurring over them has been studied only marginally [23].

In this Letter we show that network symmetries play a central role in the synchronization of a system. We consider networks of Kuramoto oscillators having identical natural frequencies, in which a phase frustration parameter forces connected nodes to maintain a finite phase difference, thus hindering the attainment of full synchronization. We prove that the configuration of phases at the stationary state depends on the symmetries of the underlying coupling network. In particular, two nodes with the same symmetry have identical phases, i.e. are fully synchronized, and this happens despite the distance of the two nodes on the graph. Such a *remote synchronization* behavior is here *induced by the network symmetries* and not by an initial ad-hoc choice of different natural frequencies [23], and can therefore be used as a method to find symmetric nodes in large complex networks.

In our model N identical oscillators are associated to the nodes of a connected graph $G(\mathcal{N}, \mathcal{L})$, with $N = |\mathcal{N}|$ nodes and $K = |\mathcal{L}|$ links. Each node i is characterized, at time t , by a phase $\theta_i(t)$ whose time evolution is governed

by the equation:

$$\dot{\theta}_i = \omega + \lambda \sum_{j=1}^N a_{ij} \sin(\theta_j - \theta_i - \alpha), \quad (1)$$

where ω is the natural frequency, identical for all the oscillators, and $A \equiv \{a_{ij}\}$ is the adjacency matrix of the graph. The model has two control parameters: $\lambda > 0$ accounting for the strength of the interaction, and α , the phase frustration parameter ranging in $[0, \pi/2]$. Kuramoto systems with frustration and heterogeneous coupling strengths have been employed to study the emergence of chimera states, i.e. of stationary states in which only a subset of the oscillators attain synchronization while the others keep drifting incoherently [24, 25].

When $\alpha = 0$, our model reduces to a network of identical Kuramoto oscillators [5, 8]. This is different from the classic case of non-identical oscillators, where the frequency distribution tends to separate the phases and, as a result, there is a transition from an incoherent state (with order parameter $r = \frac{1}{N} \left| \sum_{j=1}^N e^{i\theta_j} \right|$ equal to 0) to a synchronized one ($r \neq 0$) at a critical value λ_c of the coupling, with tightly connected nodes attaining similar phases for smaller values of λ [13, 14]. In fact, when all the oscillators have the same natural frequency, the only attractor of the dynamics is the fully synchronized state, no matter the value of λ , or the structure of the graph. Therefore, starting with random initial phases, the system will reach a fully synchronized state ($r = 1$) after a transient dynamics which reflects the structure of the graph, so that nodes belonging to the same structural module evolve similarly in time [12]. In conclusion, when $\alpha = 0$, in both the case of identical and non-identical oscillators, the nodes with similar phases will be those belonging to the same structural module.

Instead, the introduction of a phase frustration $\alpha \neq 0$ forces directly connected oscillators to maintain a constant phase difference [26]. In particular, we found that for α sufficiently small the dynamics of the model reaches a stationary state where the oscillators at two nodes with the same symmetry have exactly the same phase, and such a phase differs from the phases of nodes with different symmetries. Let us first illustrate this behavior, and the effect of the frustration parameter α with the three graphs G_a , G_b and G_c shown in Fig. 1. In Fig. 2 we report the results of the numerical integration of Eqs. (1) on the graph G_a . In the three topmost panels of Fig. 2 we plot the time evolution of the phases of the seven nodes for three values of α . We find that, after a transient, the system settles into a stationary state in which, at any time t , the phases are grouped into four different trajectories: $\theta_1(t)$, $\theta_2(t) = \theta_3(t)$, $\theta_4(t) = \theta_7(t)$ and $\theta_5(t) = \theta_6(t)$. This happens for any value of $0 < \alpha < \pi/2$, with the only difference that by increasing α we better separate the four trajectories as shown in the first three

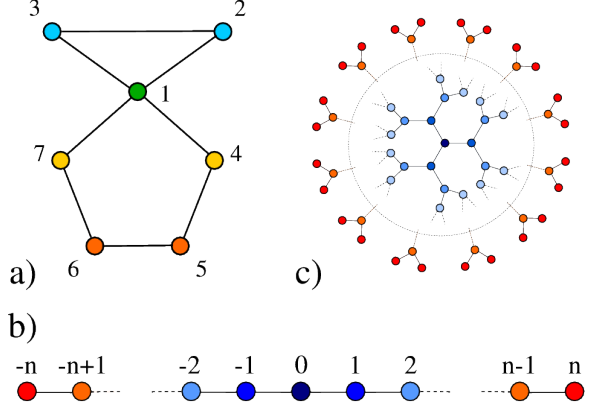


FIG. 1. (color online) The presence of frustration reveals clusters of symmetric nodes. Reported with a color code are the phases of the nodes at a given time in the stationary state. **(a)** In the first graph (G_a), node 2 is synchronized to node 3, node 4 to node 7, and node 5 to node 6. **(b)** In a finite chain (G_b), pairs of nodes symmetrically placed with respect to the central node are perfectly synchronized. **(c)** In a finite Bethe lattice (G_c) all the nodes placed at the same distance from the center have equal phases.

panels. This is confirmed by panel d), which shows the standard deviation of the oscillator phases as a function of α . The corresponding four clusters of nodes are identified by reporting with a color-code in Fig. 1 the values of the phases of the seven nodes at a given time t . We notice that each cluster groups together all the nodes with the same symmetry. In this way two distant nodes of the graph, such as for instance node 4 and node 7, are fully synchronized even if the other nodes in the paths connecting them have different phases. In this respect, what we observe is a *remote synchronization* [23] induced by network symmetries. We have found similar results for the linear chain and for the Bethe 3-lattice (see nodes with the same colors in G_b and G_c in Fig. 1).

We can explain these numerical results as follows. If α is very small, the difference $\theta_i - \theta_j$ is small for any couple of nodes i and j , and Eq. (1) can be linearized. We obtain:

$$\dot{\theta}_i = \omega - \lambda \left[\sum_{j=1}^N L_{ij} \theta_j + \alpha k_i \right] \quad (2)$$

where L_{ij} are the entries of the Laplacian matrix of the graph $L \equiv D - A$, and D is a diagonal matrix whose non-zero elements are the node degrees. Without loss of generality, we can set $\lambda = 1$, $\omega = 0$, and we can assume that at the stationary state $\dot{\theta}_i = 0, \forall i$, so that the phases must satisfy the equations $\sum_{j=1}^N L_{ij} \theta_j = \alpha [\langle k \rangle - k_i]$ at any time, or equivalently:

$$L\theta = \alpha [\langle k \rangle \mathbf{1} - \mathbf{k}] \quad (3)$$

In a connected graph the Laplacian matrix has one null eigenvalue and the system of Eqs. (3) is singular, i.e.

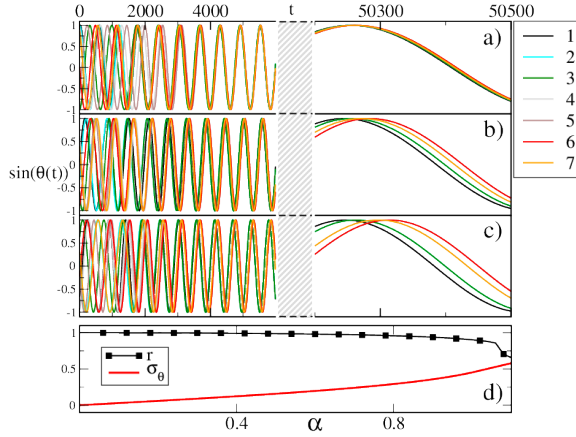


FIG. 2. (color online) After an initial transient the system is phase-locked in a stationary state where nodes with the same symmetry have the same phase. The figure refers to the graph G_a in Fig. 1a. The three top panels report three different values of the frustration parameter, respectively a) $\alpha = 0.1$, b) $\alpha = 0.5$, c) $\alpha = 0.8$, while in panel d) we show how the spreading of the phases σ_θ increases with the value of α .

it has one free variable. Consequently, at each time t we can solve the system by computing the phase difference between each node and a given node chosen as reference. For instance, for G_a , we can define the variables $\phi_j(t) = \theta_j(t) - \theta_1(t)$, $j = 2, \dots, 7$, and by solving the equations we obtain: $\phi_2 = \phi_3 = \alpha[\langle k \rangle - 2]$, $\phi_4 = \phi_7 = 2\alpha[\langle k \rangle - 2]$, and $\phi_5 = \phi_6 = 3\alpha[\langle k \rangle - 2]$. This is in agreement with the results of the simulations: in G_a the phases are clustered into four groups, with nodes with the same symmetry having the same phase, and nodes with different symmetries being separated by a phase lag that depends on α as in the relations found above. We can derive analogous analytical expressions for chain graphs and Bethe lattices. For instance, for graph G_b in Fig. 1 we obtain:

$$\theta_n - \theta_{n-i} = \theta_{-n} - \theta_{-n+i} = \left[\frac{i(i+1)}{2} \langle k \rangle - i^2 \right] \alpha \quad (4)$$

If we solve Eq. (4) for $i = n$, we obtain $\theta_n - \theta_0 = \theta_{-n} - \theta_0 = \left[\frac{n(n+1)}{2} \langle k \rangle - n^2 \right] \alpha$. Consequently, two nodes symmetrically placed with respect to node 0 will have identical phases.

We now provide a general argument to explain why the synchronization in the frustrated Kuramoto model is related to the graph symmetry. A graph $G(\mathcal{N}, \mathcal{L})$ has a symmetry if and only if it is possible to find a bijection $\pi : \mathcal{N} \rightarrow \mathcal{N}$ which preserves the adjacency relation of G , i.e. which is an automorphism for G . Formally, this means that there exists a permutation matrix $P = P(\pi)$, i.e. a matrix with each row and each column having exactly one entry equal to one and all others equal to 0),

such that $PAP^{-1} = A$. Since P is a permutation matrix, the matrix product PA swaps pairs of rows of A , while AP^{-1} swaps pairs of columns of A . Therefore, if P corresponds to an automorphism of G then PAP^{-1} actually performs a relabeling of the nodes of the original graph which preserves the adjacency matrix. This implies that P commutes with A , i.e. $PA = AP$. In general a graph can admit more than one automorphism. For instance, graph G_a in Fig. 1 has at least three non-trivial bijections which preserve the adjacency matrix, namely:

$$\begin{aligned} \pi_1 &: (1, 2, 3, 4, 5, 6, 7) \rightarrow (1, 3, 2, 4, 5, 6, 7) \\ \pi_2 &: (1, 2, 3, 4, 5, 6, 7) \rightarrow (1, 2, 3, 7, 6, 5, 4) \\ \pi_3 &: (1, 2, 3, 4, 5, 6, 7) \rightarrow (1, 3, 2, 7, 6, 5, 4) \end{aligned}$$

Node 2 and node 3 are symmetric because it is possible to find a relabeling of the nodes of G_a (e.g. by means of either π_1 or π_3) so that node 2 is mapped into node 3 and vice-versa, and the adjacency matrix of G_a is left unchanged. Similarly, for the pairs $\{4, 7\}$ and $\{5, 6\}$ we have two different relabelings (i.e. π_2 and π_3) mapping one node of each pair on the other and preserving adjacency relations. Therefore, in terms of symmetries, the graph G has four different classes of nodes: $C_1 = \{1\}$, $C_2 = \{2, 3\}$, $C_3 = \{4, 7\}$, $C_4 = \{5, 6\}$. Now, if a permutation of the nodes of a graph G is an automorphism, then $PLP^{-1} = PDP^{-1} - PAP^{-1} = D - A = L$, i.e. the associated permutation matrix P also commutes with the Laplacian matrix of the graph. If we now left-multiply both sides of Eq. (3) by P we get $PL\theta = \alpha P[\langle k \rangle \mathbf{1} - \mathbf{k}]$. Since P commutes with L and permutes symmetric nodes (notice that symmetric nodes have the same degree), then $PL = LP$ and $P\mathbf{k} = \mathbf{k}$, so we obtain:

$$LP\theta = \alpha [\langle k \rangle \mathbf{1} - \mathbf{k}] \quad (5)$$

Making use of Eq. (3) and Eq. (5) we get the linear system: $LP\theta = L\theta$. This system is singular, i.e. it has one free variable. Again, it can be solved by leaving free one of the N variables θ_i , setting $\phi_j = \theta_j - \theta_i$ and considering the new system $\tilde{L}\tilde{P}\phi = \tilde{L}\phi$. The matrix \tilde{P} is the matrix obtained from P by removing the row and the column corresponding to node i . If P does not permute node i with another node, then \tilde{P} is still a permutation matrix. Analogously, the matrix \tilde{L} is the reduced Laplacian, i.e. the non-singular matrix obtained from the Laplacian by deleting the i -th row and the i -th column. By left-multiplying by \tilde{L}^{-1} , which is not singular, we obtain:

$$\tilde{P}\phi = \phi \quad (6)$$

Since $\tilde{P}\phi$ is a permutation of the phases of symmetric nodes, Eq. (6) implies that the phases of symmetric nodes will be equal at any time, whereas by solving Eq. (5) we can get the actual values of the corresponding phases.

Application to the brain. - To investigate the functional role of symmetry in the human brain we have consid-

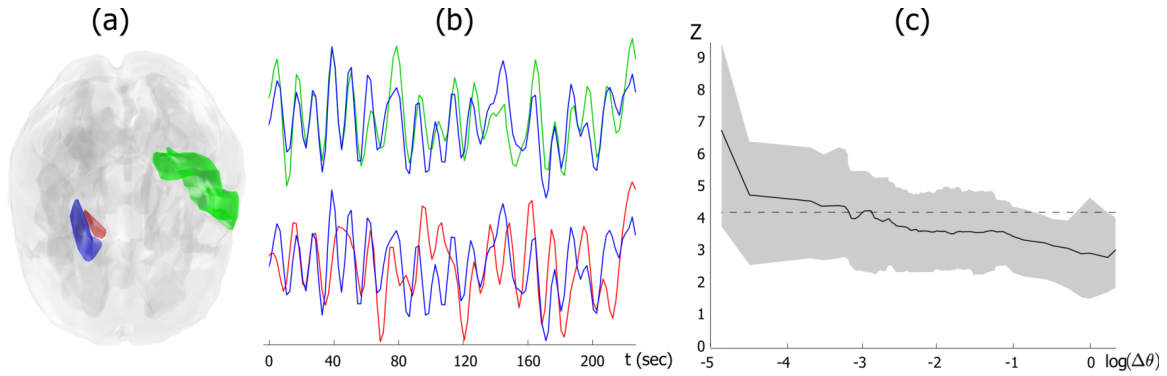


FIG. 3. (color online) (a) Brain sites with similar and dissimilar phases of the frustrated Kuramoto model are colored and superimposed onto an anatomical image. (b) Examples of functional data from one subject recorded at the brain areas indicated in plot (a). Colors are the same as those used in the anatomical image. (c) Functional correlation Z between pairs of nodes as a function of their phase differences $\Delta\theta$. Black solid curve corresponds to the average value over all the subjects, while the gray area covers the 5th and the 95th percentiles of the distribution. The dashed horizontal line indicates the threshold for statistical significant correlations ($p < 0.05$, corrected for multiple comparisons).

ered anatomical and functional brain connectivity matrices defined on the same set of $N = 90$ nodes representing different areas of the brain (see details in Appendix). We have first constructed a graph where the links represent *anatomical connectivity* as obtained from DW-MRI data [27] and used this graph as a backbone network to integrate Eq. (1). We identified candidate pairs of anatomically symmetric brain areas by means of an agglomerative clustering algorithm which groups together nodes having close phases at the stationary state (full dendrogram is reported in Fig. 4). Then, in order to assess the role of symmetry in the real activity of the brain, we have looked at the correlations between the BOLD fMRI time-series recorded during resting state on healthy individuals. We illustrate the results in Fig. 3. Consider nodes 57 and 74 corresponding respectively to green and blue areas in panel (a). Not only the two areas are spatially separated, but there is no edge connecting the two corresponding nodes in the anatomical connectivity network. However, the two nodes are detected as a candidate symmetric pair since at the stationary state of the Kuramoto dynamics in Eq. (1) the oscillators associated to these two nodes have very close phases (see dendrogram in Fig. 4). As shown in Figure 3b, we found that also the BOLD fMRI signals corresponding to nodes 57 and 74 are strongly synchronized. We obtain remarkably different results when we consider another pair of nodes, such as node 74 and node 76. These two nodes correspond to two spatially adjacent areas of the brain (the red and blue regions in Fig. 3a) and are directly connected in the anatomical connectivity network. However, at the stationary state of Eq. (1) the phase difference of the oscillators associated to node 74 and 76 is quite large. Interestingly, in this case the fMRI time-series associated to these nodes are much less similar to each other (see the two bottom trajectories reported in Fig. 3b).

To quantify this effect, we have computed the similarity between the fMRI time series associated to the nodes by means of linear correlation, followed by the Fisher's Z-transform (to stabilize the variance of the estimator) and a correction for correlated samples. In Fig. 3c we plot the average functional correlation Z between pairs of brain areas as a function the phase differences $\Delta\theta$ between the phases of the corresponding oscillators as obtained from the dynamics of Eq. (1) on the anatomical connectivity network. The fact that Z decreases with $\Delta\theta$ reveals that structural symmetry plays an important role in determining human brain functions. In fact, the functional activities of anatomically symmetric areas can be strongly correlated, even if the areas are distant in space. In this way the study of anatomical symmetries in neural systems might provide meaningful insights into the functional organization of distant brain neural assemblies during diverse cognitive or pathological states [18]. Applied to other connectivity networks as a method to detect network symmetries, our study could provide new insights on the interplay between structure and dynamics in complex systems.

The authors thank Yasser Iturria-Medina for sharing the DTI connectivity data used in the study, and Simone Severini for useful comments. M. V. acknowledges financial support from the Spanish Ministry of Science and Innovation, Juan de la Cierva Programme Ref. JCI-2010-07876. A. D-G. acknowledges support from the Spanish DGICyT Grant FIS2009-13730, from the Generalitat de Catalunya 2009SGR00838. This work was supported by the EU-LASAGNE Project, Contract No.318132 (STREP).

APPENDIX

Data acquisition and pre-processing.— The anatomical connectivity network is based on the connectivity matrix obtained by Diffusion Magnetic Resonance Imaging (DW-MRI) data from 20 healthy participants, as described in [28]. The elements of this matrix represent the probabilities of connection between the 90 anatomical regions of interest ($N = 90$ nodes in the network) of the Tzourio-Mazoyer brain atlas [29]. These probabilities are proportional to the density of fibers between different areas, so each element of the matrix represents an approximation of the connection strength between the corresponding pair of brain regions.

The functional brain connectivity was extracted from BOLD fMRI resting state recordings obtained as described in [30]. All fMRI datasets (segments of 5 minutes recorded from 15 healthy subjects) were co-registered to the anatomical dataset and normalized to the standard MNI (Montreal Neurological Institute) template image, to allow comparisons between subjects. As DW-MRI data, normalized and corrected functional scans were subsampled to the anatomical labeled template of the human brain [29]. Regional time series were estimated for each individual by averaging the fMRI time series over all voxels in each region (data were not spatially smoothed before regional parcellation). To eliminate low frequency noise (e.g. slow scanner drifts) and higher frequency artifacts from cardiac and respiratory oscillations, time-series were digitally filtered with a finite impulse response (FIR) filter with zero-phase distortion (bandwidth 0.01 – 0.1 Hz) as in [30].

Functional synchrony.— A functional link between two time series $x_i(t)$ and $x_j(t)$ (normalized to zero mean and unit variance) was defined by means of the linear cross-correlation coefficient computed as $r_{ij} = \langle x_i(t)x_j(t) \rangle$, where $\langle \cdot \rangle$ denotes the temporal average. For the sake of simplicity, we only considered here correlations at lag zero. To determine the probability that correlation values are significantly higher than what is expected from independent time series, $r_{ij}(0)$ values (denoted r_{ij}) were firstly transformed by the Fisher's Z transform

$$Z_{ij} = 0.5 \ln \left(\frac{1 + r_{ij}}{1 - r_{ij}} \right) \quad (7)$$

Under the hypothesis of independence, Z_{ij} has a normal distribution with expected value 0 and variance $1/(df - 3)$, where df is the effective number of degrees of freedom [31–33]. If the time series consist of independent measurements, df simply equals the sample size, N . Nevertheless, autocorrelated time series do not meet the assumption of independence required by the standard significance test, yielding a greater Type I error [31–33]. In presence of auto-correlated time series df must be cor-

rected by the following approximation:

$$\frac{1}{df} \approx \frac{1}{N} + \frac{2}{N} \sum_{\tau} r_{xx}(\tau) r_{jj}(\tau), \quad (8)$$

where $r_{xx}(\tau)$ is the autocorrelation of signal x at lag τ .

To estimate a threshold for statistically significative correlations, a correction for multiple testing was used. The False Discovery Rate (FDR) method was applied to each matrix of Z_{ij} values [34]. With this approach, the threshold of significance Z_{th} was set such that the expected fraction of false positives is restricted to $q \leq 0.05$.

Clustering of phase values.— To identify brain areas related by a topological symmetry, we use the anatomical connectivity obtained from the DW-MRI data as the connectivity matrix ($N = 90$ nodes) in Eq. (1). A standard hierarchical agglomerative clustering algorithm is then used to identify nodes with similar phases [35]. The resulting dendrogram is depicted in Fig. 4.

- [1] Pikovsky, A., Rosenblum, M. & Kurths, J. *Synchronization: a Universal Concept in Nonlinear Sciences* (Cambridge University Press, 2003).
- [2] S.H. Strogatz, *Nature* **410**, 268 (2001).
- [3] E. Bullmore and O. Sporns, *Nature Reviews Neuroscience* **10**, 186 (2009).
- [4] M. Chavez, M. Valencia, V. Navarro, V. Latora, and J. Martinerie, *Phys. Rev. Lett.* **104**, 118701 (2010)
- [5] Y. Kuramoto, *Lect. Notes in Physics* **30**, 420 (1975).
- [6] H. Sakaguchi and Y. Kuramoto, *Prog. Theor. Phys. Vol. 76*, 576 (1986)
- [7] S.H. Strogatz, *Physica D* **143**, 1 (2000).
- [8] J A Acebrón, L L Bonilla, C J Pérez-Vicente, F Ritort, and R Spigler, *Rev. Mod. Phys.* **77**, 137-185 (2005).
- [9] D.J. Watts and S.H. Strogatz, *Nature* **393**, 440 (1998).
- [10] S. Boccaletti, V. Latora, Y. Moreno, M. Chavez and D.-U. Hwang, *Phys. Rep.* **424**, 175 (2006).
- [11] A. Arenas, A. Díaz-Guilera, J. Kurths, Y. Moreno and C. Zhou, *Phys. Rep.* **469**, 93 (2008).
- [12] A. Arenas, A. Díaz-Guilera and C.J. Pérez-Vicente, *Phys. Rev. Lett.* **96**, 114102 (2006).
- [13] S. Boccaletti, M. Ivanchenko, A. Pluchino, V. Latora, A. Rapisarda, *Phys. Rev. E* **75**, 045102(R) (2007).
- [14] J. Gómez-Gardeñes, Y. Moreno and A. Arenas, *Phys. Rev. Lett.* **98**, 034101 (2007).
- [15] R. Gutiérrez, A. Amann, S. Assenza, J. Gómez-Gardeñes, V. Latora, S. Boccaletti, *Phys. Rev. Lett.* **107**, 234103 (2011)
- [16] L. Prignano and A. Diaz-Guilera, *Phys Rev E* **85**, 036112 (2012).
- [17] S. Fortunato, *Phys. Rep.* **486**, 75 (2010).
- [18] F. Varela, J.-P. Lachaux, E. Rodriguez and J. Martinerie, *Nat. Rev. Neurosci.* **2**, 229 (2001).
- [19] J. E. Rosenthal and G. M. Murphy, *Rev. Mod. Phys.* **8** 317 (1936).
- [20] E.M. Luks, *J. Comput. System Sci.* **25**, 42 (1982).
- [21] P. Holme, *Phys. Rev. E* **74**, 036107 (2006).

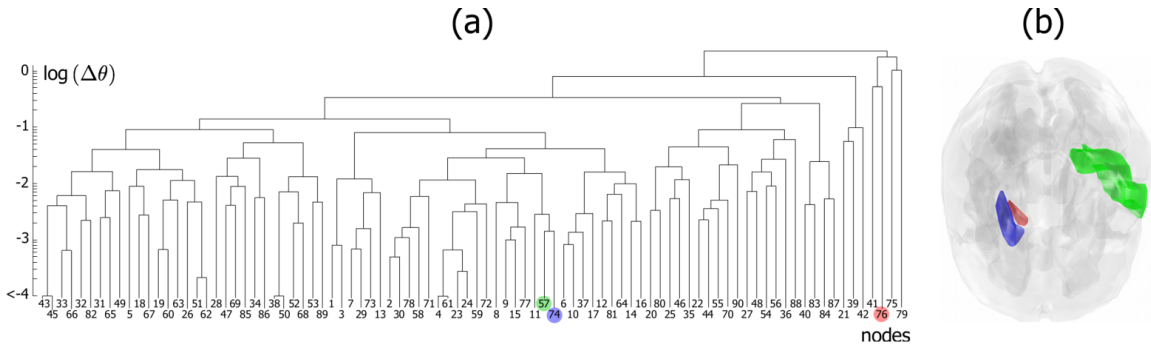


FIG. 4. Hierarchical clustering of phase values obtained from anatomical connectivity in Eq. (1). Nodes correspond to the different brain areas. Brain sites with similar and dissimilar phases are colored and superimposed onto an anatomical image.

- [22] P. Holme, Journ. of the Korean Phys. Soc. **50**, 300 (2007).
- [23] A. Bergner, M. Frasca, G. Sciuto, A. Buscarino, E. J. Ngamga, L. Fortuna, J. Kurths, Phys. Rev. **E85**, 026208 (2012).
- [24] D. M. Abrams, S. H. Strogatz, Phys. Rev. Lett. **93**, 174102 (2004).
- [25] M. Shanahan, Chaos **20**, 013108 (2010).
- [26] In general, Eqs. (1) do not admit a fully synchronized stationary state, because the system $\Omega = \dot{\theta}_i = \omega - \lambda k_i \sin \alpha \forall i$ has no solutions except for regular graphs, where $k_i = k \forall i$.
- [27] Y. Iturria-Medina, et al. Cerebral Cortex **21**, 56 (2011).
- [28] Y. Iturria-Medina, et al. Neuroimage **40**, 1064 (2008).
- [29] N. Tzourio-Mazoyer, B. Landau, D. Papathanassiou, F. Crivello, O. Etard, N. Delcroix, B. Mazoyer, and M. Joliot. Neuroimage **15**, 273 (2002).
- [30] M. Valencia, M. A. Pastor, M. A. Fernández-Seara, J. Artieda, J. Martinerie, and M. Chavez. Chaos **19**, 023119 (2009).
- [31] M. S. Bartlett J. R. Stat. Soc. B **8**, 27 (1946).
- [32] G. V. Bayley, and J. M. Hammersley J. R. Stat. Soc. B **8**, 184 (1946).
- [33] G. M. Jenkins, and D. G. Watts *Spectral analysis and its applications*. Holden-Day, San Francisco, California, (1968).
- [34] Y. Benjamini, and Y. Yekutieli, Ann Statist **29**, 1165 (2001).
- [35] G. Gan, C. Ma, and J. Wu *Data clustering: Theory, Algorithms, and Applications*. ASA-SIAM Series on Statistics and Applied Probability, SIAM, Philadelphia, ASA, Alexandria, VA, (2007).